Engineering 5 (2019) 479–489

Contents lists available at ScienceDirect

Engineering

journal homepage: www.elsevier.com/locate/eng

Research
Deep Matter & Energy—Article

Applications for Nanoscale X-ray Imaging at High Pressure

Wendy L. Mao [a,b,*], Yu Lin [b], Yijin Liu [c], Jin Liu [a]

[a] Department of Geological Sciences, Stanford University, Stanford, CA 94305, USA
[b] Stanford Institute for Materials and Energy Sciences, SLAC National Accelerator Laboratory, Menlo Park, CA 94025, USA
[c] Stanford Synchrotron Radiation Lightsource, SLAC National Accelerator Laboratory, Menlo Park, CA 94025, USA

ARTICLE INFO

Article history:
Received 9 July 2018
Revised 17 September 2018
Accepted 16 January 2019
Available online 18 March 2019

Keywords:
X-ray imaging
High pressure
Diamond anvil cell

ABSTRACT

Coupling nanoscale transmission X-ray microscopy (nanoTXM) with a diamond anvil cell (DAC) has exciting potential as a powerful three-dimensional probe for non-destructive imaging at high spatial resolution of materials under extreme conditions. In this article, we discuss current developments in high-resolution X-ray imaging and its application in high-pressure nanoTXM experiments in a DAC with third-generation synchrotron X-ray sources, including technical considerations for preparing successful measurements. We then present results from a number of recent *in situ* high-pressure measurements investigating equations of state (EOS) in amorphous or poorly crystalline materials and in pressure-induced phase transitions and electronic changes. These results illustrate the potential this technique holds for addressing a wide range of research areas, ranging from condensed matter physics and solid-state chemistry to materials science and planetary interiors. Future directions for this exciting technique and opportunities to improve its capabilities for broader application in high-pressure science are discussed.

© 2019 THE AUTHORS. Published by Elsevier LTD on behalf of Chinese Academy of Engineering and Higher Education Press Limited Company. This is an open access article under the CC BY-NC-ND license (http://creativecommons.org/licenses/by-nc-nd/4.0/).

1. Introduction

As a fundamental thermodynamic variable, pressure can be used to induce dramatic changes in materials. The ability to simulate extreme environments (like those in planetary interiors) and then characterize samples subjected to high pressure provides a powerful tool for research in fundamental physics and chemistry, as well as in more applied areas such as materials science and earth and planetary sciences; thus, advances in high-pressure science are closely tied to technological advances in analytical tools. Standard probes requiring a vacuum environment such as electron microscopy or atomic force microscopy are incompatible with *in situ* high-pressure experiments. Optical techniques can probe high-pressure samples through a transparent diamond window, but are constrained in resolution by the diffraction limit of optical wavelengths. The ability to conduct measurements *in situ* at high pressures and temperatures with nanoscale spatial resolution and improved temporal resolution would greatly enhance our understanding of materials' response to extreme conditions. *In situ* techniques are especially critical for studying non-quenchable phases or for dynamic studies in which experiments that investigate recovered samples are insufficient.

Diamond anvil cells (DACs) have found wide use for their flexibility as static compression devices that can reach very high pressures (over 750 GPa has been reported [1]). DACs can be simultaneously coupled with cryostats to reach low temperatures, or with heating techniques to reach high temperatures. In addition, the transparency of single-crystal diamond windows over a wide range of electromagnetic radiation has enabled the development of analytical probes for comprehensive, *in situ* high pressure–temperature (*P–T)* characterization. As a window, diamond is transparent below 5 eV, opaque from 5 eV to 5 keV, and then transparent again to X-rays greater than 5 keV. Synchrotron X-ray techniques offer many advantages for high-pressure DAC experiments. The exceptional brightness and penetrating power of hard X-ray synchrotron sources have made measurements that were previously flux-limited possible [2]. The short wavelength of hard X-rays also means that the resolution is not limited by the probe wavelength, but rather by the quality of the X-ray optics. This is an important consideration because due to their small sample size, DAC experiments (especially at higher pressures) require high spatial resolution to image the sample volume and internal features. The

* Corresponding author.
E-mail address: wmao@stanford.edu (W.L. Mao).

https://doi.org/10.1016/j.eng.2019.01.006
2095-8099/© 2019 THE AUTHORS. Published by Elsevier LTD on behalf of Chinese Academy of Engineering and Higher Education Press Limited Company.
This is an open access article under the CC BY-NC-ND license (http://creativecommons.org/licenses/by-nc-nd/4.0/).

development of higher (nanoscale) spatial resolution imaging represents an exciting development for high-pressure DAC studies. In the remainder of this article, Section 2 describes developments in nanoscale transmission X-ray microscopy (nanoTXM) at synchrotrons, and Section 3 describes considerations for sample preparation for DAC imaging work. Section 4 then presents examples of high-pressure applications using high-pressure synchrotron nanoscale imaging, followed by thoughts on future opportunities in Section 5.

2. Introduction to transmission X-ray microscopy

X-rays have been used for imaging since their discovery over 120 years ago [3]. Transmission X-ray microscopy (TXM) represents a powerful, non-destructive method for *in situ* imaging of the internal structure of a sample of interest. TXM radiographs are collected over many orientations and then reconstructed into a three-dimensional (3D) object through computed tomography (CT). Many X-ray imaging modalities have been developed, and various experimental setups have been engineered. These operate over different energy ranges, cover varying scale lengths, and can use different contrast mechanisms. Examples include medical and industrial CT systems that image large samples with sub-millimeter resolution [4], micro CT systems that provide sub-micron resolution over a field of view (FOV) of millimeters to centimeters [5], and nano CT systems that further reduce the spatial resolution to a few tens of nanometers for tens of micron-sized samples [6]. Although these techniques are all rooted in the same principle [7], they involve differing degrees of engineering challenges in practice. This is especially true when striving for higher spatial resolution, due to the sophisticated setup required for high-resolution X-ray microscopes [8], which involves complicated components including precision stages and fine X-ray optics [9]. The combination of an advanced X-ray source and a nanoTXM system adds complexity, but has been successfully applied at a number of synchrotron X-ray facilities around the world for applications in many research fields, such as geoscience [10], bioscience [11], energy materials [12], industrial catalysis [13], and high-pressure science (see examples in Section 4). Synchrotron facilities provide X-rays of high brightness and tunability over a wide energy range, which can facilitate more advanced X-ray imaging experiments that can offer both temporal resolution and chemical sensitivity by monitoring a sample's X-ray absorption spectrum [14].

2.1. Beamline configuration for nanoTXM

The schematic of a typical synchrotron-based nanoTXM system, such as beam line 6-2c at the Stanford Synchrotron Radiation Lightsource (SSRL), SLAC National Accelerator Laboratory, is shown in Fig. 1(a) [15]. As illustrated in the figure, the X-rays from a superconducting wiggler pass through a set of mirrors before they are focused to a spot size of a few hundred microns, which acts as the virtual source for the nanoTXM system. The monochromator selects a narrow band pass from the incident X-ray beam, providing quasi-monochromatic illumination to the downstream optics. A mirror pitch feedback system monitors micron-level beam movements and adjusts the pitch of the toroidal mirror in real time to stabilize the beam. The nanoTXM system is designed to work over an energy range from 5 to 14 keV and utilizes a capillary condenser to focus the beam to a spot of about 15 μm. To provide more flat illumination for the FOV (about 30 μm), the condenser is mechanically agitated in a plane that is perpendicular to the beam. A Fresnel zone plate is used to achieve magnifications of approximately 50× (depending on the energy configuration of the incident X-rays), which is further increased by 10×–20× using an optical objective lens that is downstream of the scintillator crystal. A charge-coupled device (CCD) coupled with the scintillator crystal collects the projected images. The spatial resolution of this system is about 30 nm, which is confirmed by a calibration pattern (Fig. 1). The sample stage offers six independent motions including, from the bottom to the top, the 3D (x, y, z) translation stage, a rotation (θ) stage, and a two-dimensional (2D) (x, z) translation stage. The 2D translation stage on top is used to bring the sample to the rotation center in order to ensure that the sample stays within the FOV as it is rotated. The rotation stage facilitates the acquisition of projection images of the sample at different viewing angles, which are then reconstructed into a 3D matrix that represents the 3D structure of the sample.

2.2. Requirements for high-pressure nanoTXM

Although a significant amount of effort has been devoted to the design of compact DACs, the cell structure still requires sufficient working distance to accommodate the DAC in the experimental setup. The focal length of a Fresnel zone plate is a function of the X-ray energy. Higher X-ray energy results in a longer focal length and, thus, in a longer working distance. Considering the requirements for penetration capability and working distance, it is only feasible to use hard X-rays to access samples subjected to high pressure. Certain systems of interest that do not contain heavy elements or elements with a suitable absorption edge can have poor X-ray absorption contrast, limiting the use of conventional bright-fielding imaging. The DAC also causes missing angles, in which the X-ray is blocked by the mechanical support posts. These practical challenges complicate the experiments and subsequent data analysis. Here, we present some recent technical developments that target some of these challenges; Section 4 provides more detailed discussion of specific scientific case studies.

2.3. Data collection and analysis for high-pressure nanoTXM

During nanoTXM data acquisition, images without the sample are needed as reference images for flat-field background removal through application of the Beer–Lambert law. The reference images are usually acquired before and after the angular scan. In some cases, reference images are collected more often to account for any background variation due to the instability of the system. Depending on the design of the experiment—and, in particular, on the image contrast and signal-to-noise ratio—multiple images may be taken at the same viewing angle. The data acquisition macro is defined to take into account these factors, together with other practical limitations such as the amount of available beam time for a particular experiment. A typical macro for a tomographic scan involves thousands of motor movements and hundreds of image-acquisition commands. The macro for executing a spectroscopic tomography scan can be even more complicated, with the number of command lines potentially increasing by a few orders of magnitude. In practice, it is impossible to manually conduct the data collection for such experiments. We have developed software tools to construct sophisticated macros based upon specific experiments designed by the user. These tools for advanced imaging system control are freely available in TXM-Wizard, a software package developed at SSRL [17].

The macros described above execute complex experiments automatically and generate a large amount of imaging data. When running at full speed, over a terabyte of raw data can be produced in one week. Data processing generates even more files, resulting in further challenges in terms of data management. In addition to the challenges of handing data volume, the nanoTXM data themselves are information-rich and complex. Next, we discuss some of

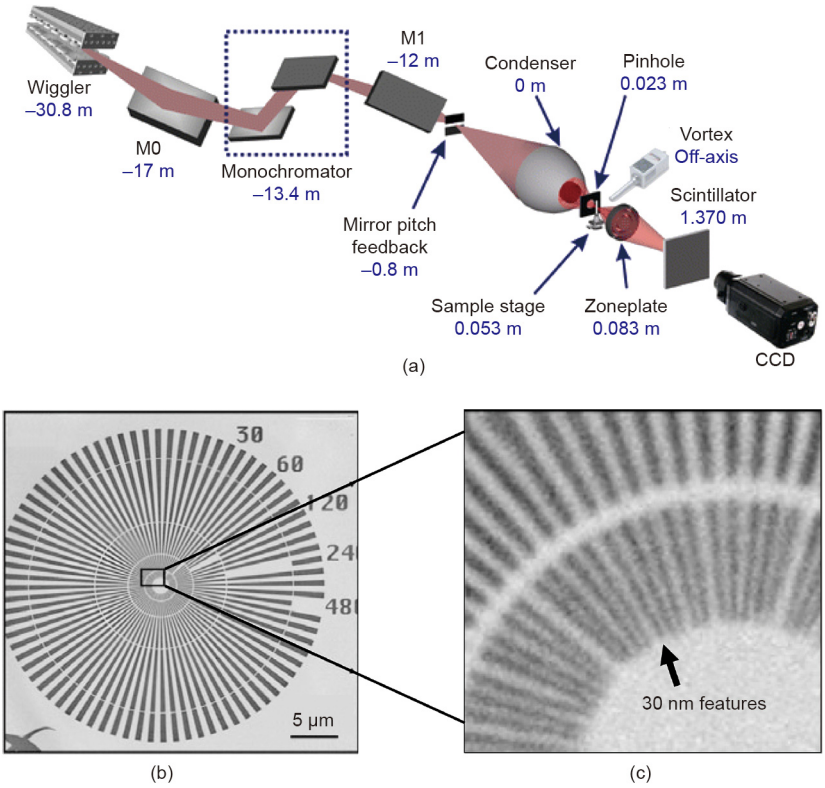

Fig. 1. (a) Schematic experimental setup of the TXM installed at the SSRL beam line 6-2c; (b, c) transmission image of a resolution target. M: mirror. (a) Reproduced from Ref. [15] with permission of Springer-Verlag, © 2012; (b, c) reproduced from Ref. [16] with permission of Microscopy Society of America, © 2010.

the issues to consider in the data analysis of high-pressure nanoTXM data.

2.3.1. Motor jitter correction

During tomographic data acquisition, the sample is rotated along an axis perpendicular to the incoming X-ray beam. In an ideal setup, the rotation axis is projected to the central column of the detector—this is, however, often not the case in practice. Prior to the tomographic reconstruction, it is important to identify the center of rotation with respect to the projection images. The static translational and rotational image offset can be determined and corrected using a number of different methods [18–20]. In the case of nanoTXM, alignment of the projection images is more challenging. When trying to image with nanoscale resolution, mechanical imperfections in the imaging system become clearly detectable, which results in random jitters in the projection images. Proper corrections that compensate for the image jitter are needed to prevent the introduction of image artifacts in the reconstructed 3D volume, which would significantly degrade the quality of the reconstruction. Traditionally, manual alignment of the projection images is carried out to prepare the dataset for tomographic reconstruction; however, such alignment has very limited precision and is inefficient.

Based on the concept of "tomographic consistency" [21,22], we have developed an iterative method to conduct projection image alignment in an automatic manner [23]. In this method, we register the experimentally measured projection images to the images that are numerically calculated by re-projecting the 3D matrix. Several image-registration algorithms are implemented and executed in a designed sequence. The quality of the reconstruction is significantly improved without human interaction. This method is readily applicable to high-pressure applications, and particularly to spectroscopic tomography, which involves energy scans.

2.3.2. Missing angle

For tomographic scans, the more angles at which the object is imaged (where complete sampling would be 180°), the better the information that is obtained. A DAC includes posts that must be strong enough to support the cell as the opposing diamond anvils are advanced against each other. These posts block X-rays and prevent imaging over a certain angular range (Fig. 2). For two-post panoramic DACs [2], which are used in high-pressure studies where the X-rays are directed perpendicular to the compression axis (e.g., radial X-ray diffraction (XRD) and a number of X-ray spectroscopies), the opening angle is approximately 135°, which leaves about 45° inaccessible for imaging. For four-post cross DACs [24], which are designed with wider radial access, an angular access of up to 152° has been achieved by the use of thinned posts,

Fig. 2. (a) Two-post panoramic DAC; (b) four-post cross DAC. The X-ray beam is directed perpendicular to the compression axis along the radial opening.

while still maintaining sufficient support for reaching high pressures. In the case of the cross DAC design, another advantage is that the missing angle is divided into two sections separated by 90°, making the artifacts caused by missing angles less severe. Since complete 180-degree access is impossible with current DAC environments, direct reconstruction of incomplete angle sampling results in uncertainty in the volume or morphology determination. To overcome this problem, we have developed and applied an iterative reconstruction algorithm—the algebraic reconstruction technique (ART)—to reduce the artifacts caused by an incomplete dataset and to improve the quality of 3D tomography data [25].

2.3.3. Quantification of the imaging data

The efforts described above have resulted in dramatic improvements in the quality of 3D reconstructions, which are crucial for optimizing the accuracy and fidelity of the quantification of imaging data. For example, quantification of sample volume as a function of pressure can be used to determine the equation of state of amorphous or poorly crystalline samples, and the evaluation of the volume fraction of different material phases, their microscopic spatial distribution, and their phase boundaries is extremely valuable for understanding the evolution of pressure-induced phase transitions (see Section 4 for examples). The quality of these detailed analyses relies on the accuracy of the reconstructed 3D volume, which is a starting point for a more comprehensive interpretation of the data. A more detailed discussion about imaging data quantification can be found in review articles [6].

2.3.4. Data mining in spectroscopic tomography

The combination of a nanoTXM system with a synchrotron X-ray facility has opened up exciting opportunities beyond those available for laboratory X-ray sources. One of the major advantages of using a synchrotron source is the ability to resolve material phases with different spectroscopic fingerprints. Compared with the standard bulk X-ray spectroscopy technique, the use of an area detector in a nanoTXM system increases the data rate by nearly six orders of magnitude. After data reduction, each volume unit of about 30 nm × 30 nm × 30 nm is associated with a unique X-ray absorption spectrum. Thanks to our technical developments, which are described above and elsewhere [17], data reduction is no longer a bottleneck for processing. It is, however, still not a straightforward process to extract scientifically important information from the data.

When sufficient prior knowledge of the system is available, a supervised machine learning approach can be used to interpret the data. For example, if we know the spectra for both the parent phase and the new phase, we can determine the spatial distribution of these phases by quantifying the similarity in the spectra. Such a supervised approach is both effective and efficient, and has been successfully applied to high-pressure research [24]. The reliance on the prior knowledge of the system is, however, a major limitation of the supervised approach. In more complex systems, there are often minor phases that play important roles in affecting the overall behavior of the system. These minor phases can be both small in population and sparse in spatial distribution. They are often also unknown, which means that they cannot be included in a supervised search. It is of fundamental and practical importance to be able to identify and study these minor phases. We have used unsupervised machine learning approaches, such as unsupervised clustering methods, to search for hidden information in big data [26,27]. This approach could facilitate the identification and visualization of nucleation points in a material that undergoes a pressure-induced phase transition. It could also help capture intermediate phases that are metastable but could be critically important for understanding transition pathways.

2.3.5. Data visualization

While the quantification of the imaging data is often the ultimate goal, rapid and accurate visual presentation of the data is very desirable because it offers a "seeing is believing" way of studying, understanding, and interpreting the result. Advanced tools are certainly needed for visualization of the X-ray tomographic data, which is large in its volume and complex in its structure. Depending on the specific application, many different visualization modules are desired. Examples include but are not limited to ① virtual slicing through different orientations and depths; ② volume rendering with color coding to user-defined color maps; ③ extraction and visualization of 2D iso-contours or 3D iso-surfaces; and ④ visualization of 3D vector maps. These functionalities have been independently developed and are available in many well-established software packages.

The most popular open-source software platform for tomographic data visualization is probably ImageJ, which allows individuals to contribute different plugins and which has formed a useful library. Users can find most of the desired functionalities in the ImageJ platform for direct use or for modification/extension. On the other hand, commercial software packages including Avizo®, Amira® (Field Electron and Ion Company, USA), and Dragonfly (Object Research Systems Inc., Canada) are very powerful and user-friendly. They provide a useful set of tools for data preparation, visualization, quantification, and modeling. It is worth mentioning that some commercial software offers different editions that target different fields of application. For example, Amira® has a strong emphasis on the life sciences, while Avizo® has different versions that focus on materials science, natural sciences, and industrial inspection, respectively.

3. Sample preparation for high-pressure nanoTXM experiments

For high-pressure nanoTXM experiments, sample preparation is crucial; several important factors that need to be considered include sample size, geometric shape, and surface smoothness. The sample size should ideally fit within the FOV so that one projection can cover the entire sample. The FOV is usually between 25 and 35 μm, depending on the energy of the incident X-ray beam, the detector size, and the spatial resolution of each pixel in the 2D projection images. When the sample size is greater than the FOV, two or more projections must be collected and then stitched together to image the whole sample at a given angle. The stitching procedure can introduce extra uncertainty into the volume determination. The sample shape can also affect the accuracy of the volume determination. The edges of the sample in the 2D projection images are more readily recognized for a regular shape, such as spheres, cubes, or cylinders. Similarly, the smoother the surface of the sample, the more accurate the 3D volume rendering will be. These three considerations can be resolved via micro machining of the sample using a focused ion beam (FIB) [28,29]. Cleaning cross-sectioning can be applied to improve the surface of the fabricated sample. To expedite the FIB milling, it is possible to first thin down the sample to the targeted thickness of 10–20 μm by polishing both sides using a very fine abrasive (Fig. 3).

For data acquisition in nanoTXM measurements, X-ray absorption contrast must be taken into account. The contrast can be maximized with the selection of the energy of the incident X-ray beam being fixed above the absorption edge of an element in the sample, such as 7.08 keV for iron and 11.12 keV for germanium [28]. In general, successful volume rendering requires transmission of about 10%–40% of the X-rays through the sample. However, if the sample is composed of only low-*Z* elements (e.g., glassy carbon), the contrast can be too low to make boundary definition in 2D

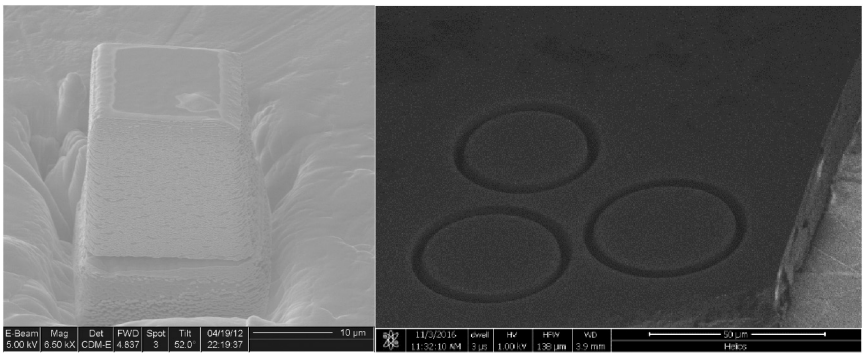

Fig. 3. Scanning electron microscope (SEM) images of silica glass samples. (a) Fabrication of a cube of approximately 15 × 15 × 15 μm^3; the cube sample was then coated with about 1.5 μm thick layer of Pt using a FIB. (b) After the silica layer was double polished down to about 16 μm thick, samples were fabricated into a cylinder shape 36 μm in diameter.

projection images feasible. It is possible to improve X-ray absorption contrast to some extent by enlarging the sample dimensions. Meanwhile, the FOV must be increased accordingly in order to capture the entire sample in one projection, which entails a compromise on spatial resolution. Alternatively, coating the sample with heavy elements can be considered in order to enhance the absorption contrast. In practice, a thin layer of platinum (Pt) (about 1 μm) can be deposited onto the surface of the sample using FIB, which increases the absorption contrast by approximately 70% at 7 keV (Fig. 3). Obtaining complete coverage of the sample can be a challenge; it is necessary to be mindful of whether the coating will affect how the sample deforms.

For high-pressure experiments in a panoramic or cross DAC, the sample, together with a pressure calibrant (e.g., a ruby ball) and a pressure-transmitting medium, are loaded into a sample chamber drilled in an X-ray transparent gasket (e.g., a beryllium (Be) gasket) because, as noted before, incident X-rays are directed onto the sample through the opening in the DAC in the radial direction (Fig. 4). Gold spheres of typically less than 1 μm in diameter can be loaded next to the sample and used as markers to facilitate alignment of the 2D images. The density contrast between the sample and the pressure-transmitting medium is critical for successful nanoTXM measurements. Silicone oil or light mineral oil is commonly used as a pressure-transmitting media to achieve a relatively high density contrast. The use of a cubic boron nitride (cBN) insert within a Be gasket helps to maintain a relatively thick sample chamber (e.g., > 30 μm up to 20 GPa), which is indispensable for ultra-high-pressure X-ray imaging measurements aimed at over 100 GPa.

4. Applications and examples

4.1. Equations of state

One application for *in situ* high-pressure nanoTXM is the determination of equations of state (EOS), which is particularly useful for amorphous or poorly crystallized materials. Due to their lack of long-range order, the XRD patterns from amorphous and liquid phases are particularly challenging to interpret, and the position of broad diffraction maxima cannot be directly related to macroscopic density. Imaging techniques for direct measurements of volume changes have been explored previously for samples at high pressure. Using X-ray tomography with micron-scale resolution, Liu et al. [30] developed a method to directly measure density by reconstructing linear absorption coefficients at varying pressures and applied it to a study of amorphous selenium (Se) under high pressure. For a typical DAC sample with dimensions of about 100 μm × 100 μm × 100 μm, a spatial resolution of 1 μm only provides uncertainties in volume at the percent level, which are an order of magnitude lower than the uncertainties from XRD of crystalline materials. At higher pressures (> 10 GPa) when the sample thickness becomes dramatically reduced to tens of microns or less, micron-resolution tomography does not provide volume measurements with sufficient accuracy. NanoTXM, which has a spatial resolution of tens of nanometers, enables volume measurements with an accuracy that rivals that of XRD of crystals; thus, it opens up exciting opportunities for high-pressure research.

As a benchmark for establishing the utility of nanoTXM for EOS determination, the volume change for a crystalline tin (Sn) sample

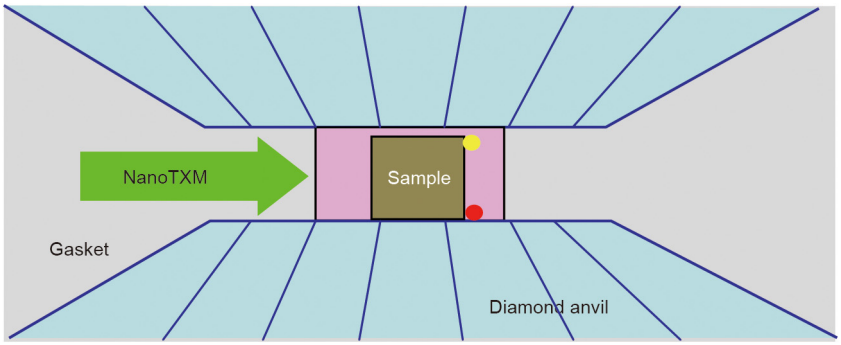

Fig. 4. Schematic drawing of sample chamber drilled inside an X-ray transparent gasket. Sample (about 30 μm cube) is surrounded by pressure medium (pink). Ruby ball (red) and gold sphere (yellow) are added as a pressure calibrant and an alignment marker, respectively.

with increasing pressure was determined in a DAC [25]. The nanoTXM gave the same results as XRD and had comparable error bars. Below, we discuss in more detail a few examples that demonstrate the potential of this method and its application for a wide variety of amorphous and poorly crystalline phases.

4.1.1. g-GeO_2

As a classic network-forming oxide glass, the structure of germania (g-GeO_2) consists of a 3D network of corner-shared GeO_4 tetrahedra. Understanding the structural, physical, and chemical properties of germania, especially the previously observed pressure-induced amorphous–amorphous transition (AAT), has implications for improving glass theory, exploring polyamorphism in amorphous materials, and advancing materials design. Although considerable experimental and theoretical efforts have been devoted to understanding the nature of the AAT, the structural information that has been accessed is limited to nearest neighbor distances and average coordination number. The determination of key macroscopic physical quantities such as density, which are essential in describing the EOS and understanding the densification process, has been elusive, in part due to technological challenges.

g-GeO_2 is an ideal candidate for high-pressure nanoTXM measurements since the Ge $K_{\beta1}$ absorption edge can be used to maximize the X-ray absorption contrast [28]. A g-GeO_2 slab was cut into a cube with the approximate dimensions of 40 μm × 40 μm × 40 μm using a FIB, and all six faces of the block were finely polished for good surface quality. A cross DAC with an X-ray transparent Be gasket with a cBN gasket insert was used to confine the sample at high pressure. The pressure–volume data of g-GeO_2 up to almost 40 GPa show a continuous increase in density, indicating that the structural transformation is a gradual process. A transition is observed between 10 and 13 GPa, above and below which germania displays distinct compressional behavior. An EOS representing tetrahedrally coordinated g-GeO_2 fits pressures up to 10 GPa, whereas the system is found to be in a different state with new elastic properties at pressures above 13 GPa (Fig. 5). g-GeO_2 may not be fully six-coordinated even up to 40 GPa, the highest pressure in the study. This is the first demonstration using nanoTXM on amorphous systems to provide a direct measurement of the volume—that is, density—of a dense solid sample *in situ* as a function of pressure.

4.1.2. Bulk metallic glasses

Bulk metallic glasses (BMGs), which are amorphous alloys composed of metal elements, are widely studied engineering materials due to their superior mechanical properties, such as high strength, fracture toughness, hardness, wear resistance, and elastic limit. These exceptional features are attributed in part to their unique atomic-packing scheme, non-directional metallic bonding, and the absence of the well-defined dislocation defects that are present in crystalline alloys. Development of BMGs with good glass-forming ability is a primary driver in the BMG research community and defining general rules for understanding what controls these materials' properties is essential to the design of new, improved BMGs.

Density is a fundamental material property that is controlled by interatomic distances and the packing of microscopic constituents. BMGs, which are isotropic and disordered, are believed to have very efficient and dense atomic packing, and their volume is expected to scale as a power of three of the average interatomic distance. As defined by the well-known Ehrenfest relationship and observed in many experiments, the average interatomic distance is inversely proportional to the position of the principal diffraction peak (q_1), which is a direct structural measurement in BMGs at the atomic level. Therefore, the expectation is that the density of BMGs will scale with the position of q_1 cubed (i.e. the power law with an exponent of three).

However, upon coupling nanoTXM with XRD, we found that the density of all of the BMGs we studied scales with a 2.5 power of their principal diffraction peak position, instead of the expected cubic relationship (Fig. 6). This 2.5 power law not only holds for BMGs with different compositions [29], but also persists even when the BMG undergoes a first-order pressure-induced polyamorphic transition [31], which suggests that it is a universal feature of BMGs and a general rule defining the structures of BMGs [32].

4.1.3. Glassy carbon

The above examples demonstrate the use of high-pressure nanoTXM to probe amorphous systems that contain heavy elements or elements with absorption edges that fall within the working energy ranges for specific synchrotron beam lines. For systems that are weakly X-ray absorbing (i.e., mainly composed of low-*Z*

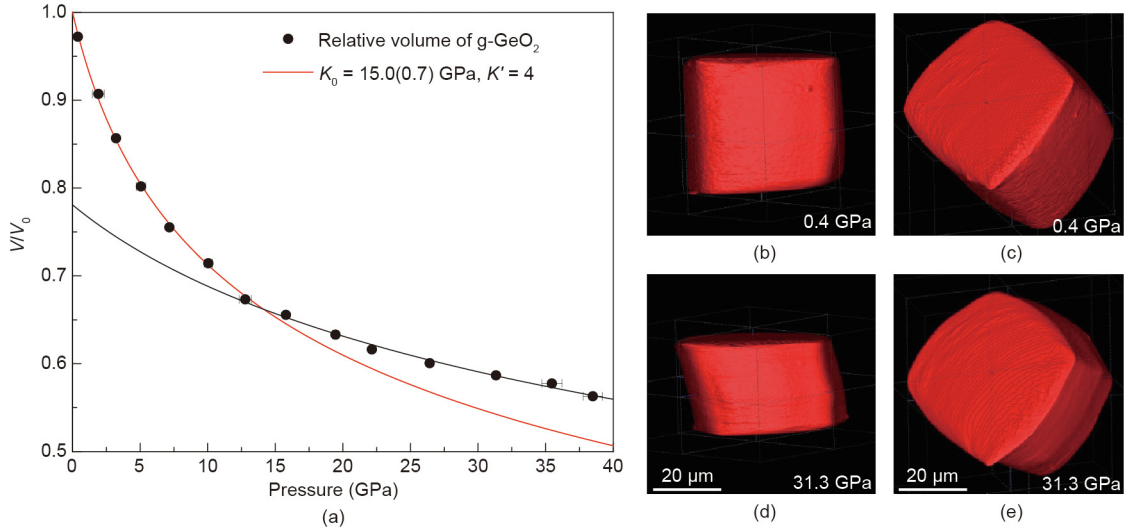

Fig. 5. (a) Normalized volume (V/V_0) change of germania glass as a function of pressure at room temperature. The EOS is shown in red solid line, while a second *P*–*V* curve (black line) covers the remaining points up to the highest pressure of this study. The error bar associated with the relative volume change is determined to be below 1%. (b–e) 3D renderings of the germania sample shown for two pressures. For (b, d), the viewing angle is almost parallel to the diamond culet plane. For (c, e), the viewing angle is titled to show more of the top of the sample. Reproduced from Ref. [28] with permission of AIP Publishing, © 2013.

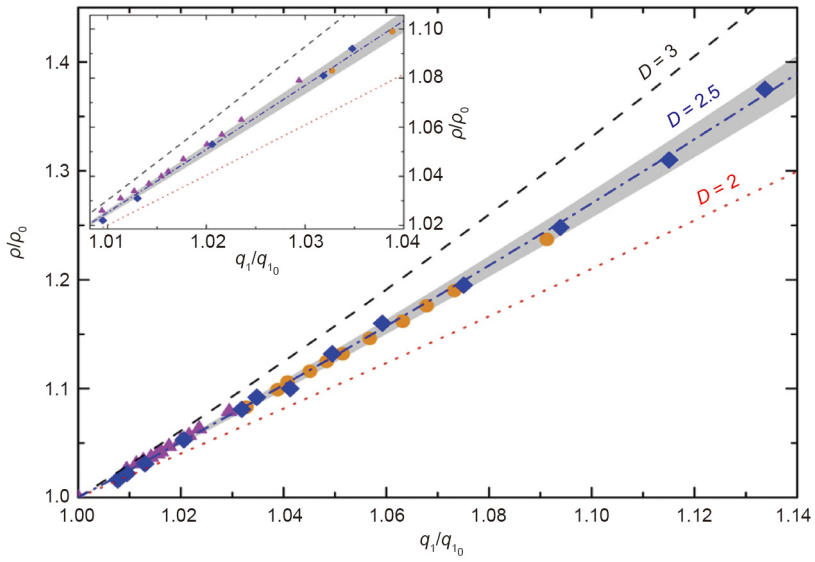

Fig. 6. Relationship between the normalized density (ρ/ρ_0) and the position of the principal diffraction peak (q_1) for $La_{62}Al_{14}Cu_{11.7}Ag_{2.3}Ni_5Co_5$ metallic glass demonstrating a surprising 2.5 power law.

elements), we have developed an imaging approach that utilizes negative absorption contrast. For example, carbon forms a variety of stable and metastable crystalline and amorphous phases with exceptional physical and chemical properties. The synthesis and study of new carbon phases have long been a rich and active research area. By compressing glassy carbon at room temperature above 40 GPa, we previously reported a new carbon allotrope we called "amorphous diamond" [33]. This carbon phase possesses a fully sp^3-bonded, amorphous structure and exceptional hardness comparable to that of a diamond, as probed by X-ray Raman scattering and XRD, which opens up exciting possibilities for application as a superhard, amorphous solid.

To better understand the glassy-carbon-to-amorphous-diamond transition, we conducted a correlation study between the microscopic structural features and macroscopic attributes such as density. Density measurements for glassy carbon as a function of pressure pose a significant technological challenge, since carbon is largely X-ray transparent. To overcome this challenge, we coated a glassy carbon sphere with a layer of X-ray absorbing material (in this case, an about 1 μm thick coating of Pt) to create sufficient absorption contrast, and then imaged the boundary between this layer and the glassy carbon sample. The "hollow" space encased by the Pt layer then defined the volume of the carbon subject (Fig. 7). We collected nanoTXM measurements on glassy carbon at various pressures upon both compression up to over 40 GPa and decompression. The EOS for the glassy-carbon-to-amorphous-diamond transformation provides us with critical constraints for modeling the glass structure and aids us in understanding the relationship between the microscopic properties and macroscopic behavior of this disordered material system.

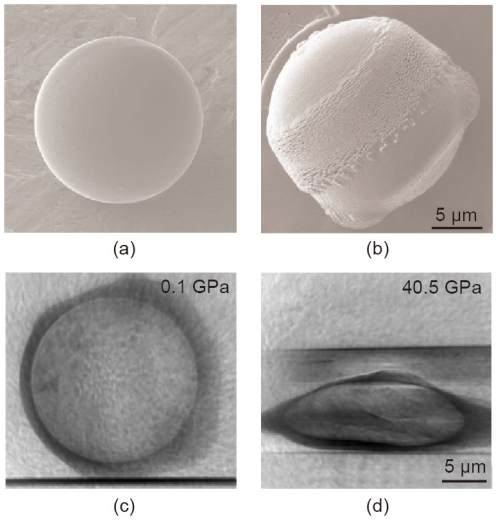

Fig. 7. SEM images of a glassy carbon sphere before (a) and after (b) a Pt coating was deposited in order to provide absorption contrast. NanoTXM radiographs at low (c) and high (d) pressure of the Pt-coated glassy carbon sample being compressed in a DAC (horizontal edges in 40.5 GPa image show diamond culets coming together).

4.1.4. g-SiO_2

SiO_2 is another low-Z material; it is also a major constituent of solid and/or molten silicate phases within the terrestrial planets and an important technological material. Silicate melts play a key role in the differentiation of the mantle and core in early-Earth and present-day mantle dynamics. Silica and silicate glasses have been used as analogs for understanding the behaviors of silicate melts under high P–T conditions because they exhibit similar microscopic and macroscopic properties [34–36]. Silica glass has been extensively studied through simulations and experiments, including XRD, X-ray Raman scattering, Brillouin light scattering (BLS), infrared absorption, optical microscopy, and X-ray absorption (e.g., Refs. [37–44]). A large discrepancy in density has been reported between X-ray absorption and BLS measurements using DACs, which suggests that the density of basalt and silicate glasses from high-pressure BLS measurements might be underestimated [36,45]. We note that BLS only probes elastic contributions to the compressibility without considering configurational contributions, given the use of the unrelaxed acoustic wave velocities [36,46]. On the other hand, the X-ray absorption technique is based on the attenuation of X-rays through a path length, assuming that the local deformation of anvils is negligible and that the mass absorption coefficient of anvils is constant within the culet at high pressures [40].

Since nanoTXM allows for direct determination of the volume of a sample at high pressure without the aforementioned assumptions and limitations, it is an ideal approach to measure the volume

(and therefore density) evolution of silica glass as a function of pressure. We investigated the EOS of silica glass at room temperature using nanoTXM combined with a cross DAC. The density of silica glass monotonically increases upon compression, with a dramatic reduction in the pressure dependence of density around 20–30 GPa (Fig. 8). The change in compressibility is likely associated with a pressure-induced structural change from tetrahedral to octahedral coordination. A comparison of the literature results on enstatite glass [36] indicates that silica glass becomes denser above 35–40 GPa due to its higher compressibility between 10 and 30 GPa. These results demonstrate that the identity and quantity of metal cations incorporated into silicate melts had an influence on the evolution of a deep magma ocean in the early Earth.

It is important to reiterate that this negative absorption contrast imaging approach has its limitations. It can only be applied to samples that can maintain a single, solid form. The additional coating step also introduces complexity and experimental uncertainties. Upon compression, the integrity of both the object of interest and the coating layer must be preserved in order to enable accurate imaging of their interface. To make more direct 3D imaging measurements on a wider array of systems consisting of low-*Z* elements, other imaging approaches must be explored, as we will discuss in Section 5.

4.2. Spectroscopic imaging

The tunability of the incident X-ray energy from a synchrotron source enables the quantitative visualization of chemical species and valence states of materials *in situ*. By performing X-ray absorption near-edge spectroscopy (XANES) 3D tomography as a function of pressure, real-time chemical and elemental mapping information with up to 30 nm spatial resolution can be quantitatively constructed. This provides a rare opportunity to understand the mechanisms of pressure-induced phase growth, phase boundary transformations, the formation of domains, or charge transfer dynamics *in situ* and *in operando*.

We realized the first such application by visualizing the phase transition in a $BiNiO_3$ powder sample at high pressure [24]. $BiNiO_3$ undergoes a gradual pressure-induced phase transition associated with the intermetallic charge transfer between bismuth (Bi) and nickel (Ni) ions. The use of *in situ* 3D spectroscopic tomography at the Ni absorption edge under varying pressures makes it possible to visualize grain boundary disappearance and growth as the low-pressure phase transforms into the high-pressure phase, from which we can investigate the phase transition mechanism and boundary dynamics (Fig. 9). This powerful five-dimensional (*x*, *y*, *z*, energy, and pressure) imaging approach can be widely applied to systems that undergo pressure-induced chemical or physical processes that involve oxidation state changes, charge transfer, and spin transitions. Detailed quantitative analysis can provide significant insight into the mechanisms associated with these processes, which contribute to structural, optical, electronic, and/or magnetic transitions.

We are currently improving the high-pressure spectroscopic nanoTXM capability to enable XANES 3D nanotomography with higher energy resolution and faster data collection (3–5 min per tomography). These improvements will allow higher quality 3D XANES measurements that can be used for phase transition dynamics studies associated with the interplay of strongly intertwined lattice, charge, and spin degrees of freedom in complex systems. We are also shifting our focus to single-crystal samples, for which more accurate quantitative measurement and analysis can be performed.

5. Future prospects

With the current capabilities on hand, there are still materials systems to be explored using high-pressure nanoTXM. Further developments in improving this technique make the future very bright for research in this area. Below, we note just a few of the exciting directions that are currently being explored.

5.1. Combining high temperature with high pressure

All previous and current high-pressure nanoTXM experiments have been and are being performed at room temperature. The

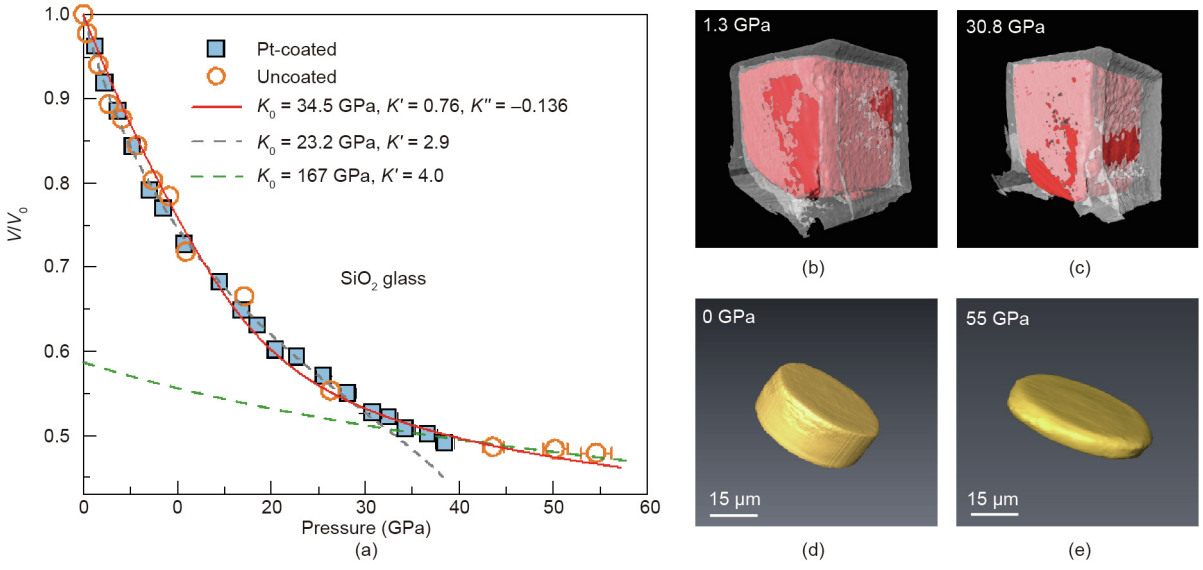

Fig. 8. (a) Normalized volume change of silica glass as a function of pressure at room temperature. Solid and empty symbols represent nanoTXM measurements for the Pt-coated and uncoated samples, respectively; solid curve shows a fourth-order Birch–Murnaghan EOS fit to the entire pressure range from 0 to 55 GPa; dashed gray curve shows a third-order BM EOS fit between 0 and 30 GPa; dashed green curve shows a second-order BM EOS fit between 35 and 55 GPa. The error bar associated with the relative volume change is determined to be below 1%, which is smaller than the symbol size. (b, c) show representative 3D renderings from a high-pressure nanoTXM experiment on the Pt-coated SiO_2 cube shown in Fig. 4. The Pt coating is shown in gray and the "hollow" volume representing the SiO_2 cube is shown in red. The volume has decreased by a factor of two, from 1.3 to 30.8 GPa. (d, e) show representative 3D renderings from a high-pressure nanoTXM experiment on the SiO_2 cylinder shown in Fig. 4.

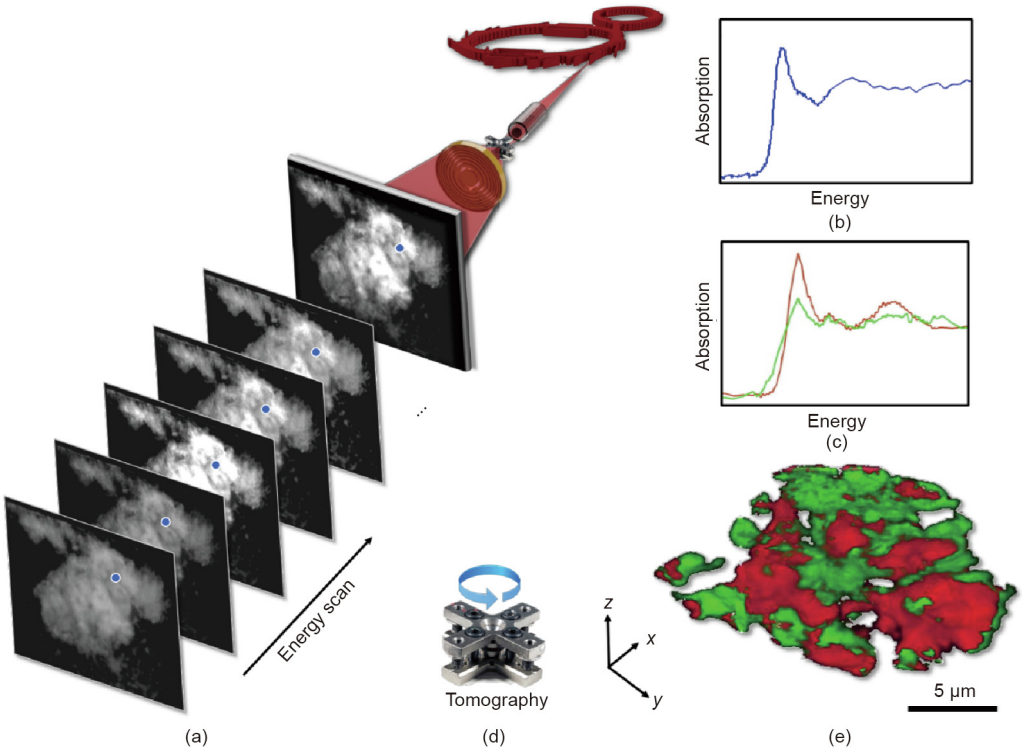

Fig. 9. Illustration of synchrotron-based spectro-microscopy under high pressure. (a) Schematic of the experimental configuration and data structure. A series of transmission images are acquired using the 2D area detector as a function of the incoming X-ray energy. (b) Extraction of the local XANES spectrum associated with the blue pixel highlighted in (a). The extracted XANES spectrum in (b) is fit using known standards (c) for quantification of the local oxidation state. (d) The tomographic scan, in which the DAC is rotated along an axis that is perpendicular to the X-rays. (e) Combining 2D spectro-microscopy with tomography, 3D phase separation in the sample can be resolved. This phase separation can be monitored as the external pressure is tuned, revealing the nucleation and the propagation of the pressure-driven phase transition in the material [24].

capability to expand nanoTXM to a much wider *P*–*T* space by adding variable temperature is desirable for a variety of applications. Resistive and laser-heating techniques coupled with high-pressure apparatus have been widely applied in many optical, transport measurements, and XRD and spectroscopy studies. To enable high-pressure/high-temperature nanoTXM, previous experiences—especially those related to high-pressure and high-temperature radial XRD—will guide our experimental design, and a similar setup geometry can be implemented (Fig. 10). With the appropriate selection of gasket materials and resistive heaters, the current cross DAC that is used for room-temperature nanoTXM measurements can be used to access temperatures up to 1000 K. To reach higher temperatures, one possible solution would be to couple a single-sided fiber laser with a high-pressure nanoTXM DAC.

5.2. Phase contrast imaging

To overcome the limitations imposed by bright-field imaging with negative absorption contrast, and to be able to directly visualize systems consisting of low-*Z* elements with hard X-rays, the development of propagation-based phase contrast imaging for high-pressure samples represents a future direction (Fig. 11). The high-pressure sample of interest will be placed out of the zone-plate (ZP) in-focus plane, and a set of defocused images will be recorded. The free-space propagation from the sample position to the ZP focal plane results in Fresnel diffraction patterns that contain the phase distortion information induced by the sample. Advanced phase-retrieval algorithms that are applicable to the ZP-based nanoTXM system will be used to retrieve the quantitative phase information. Although we have been designing DACs with as

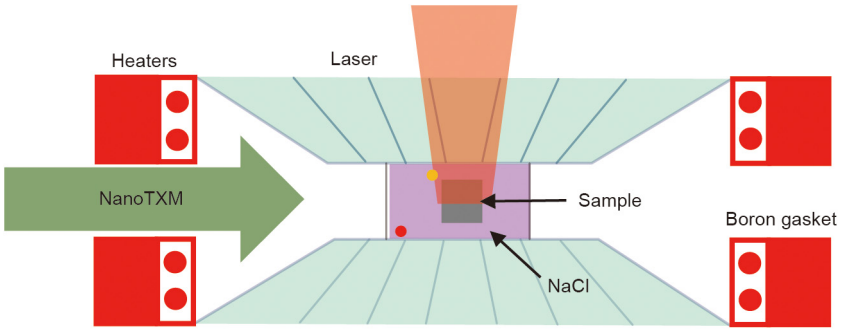

Fig. 10. Schematic drawing showing the addition of resistive heating or single-sided laser heating capabilities to nanoTXM.

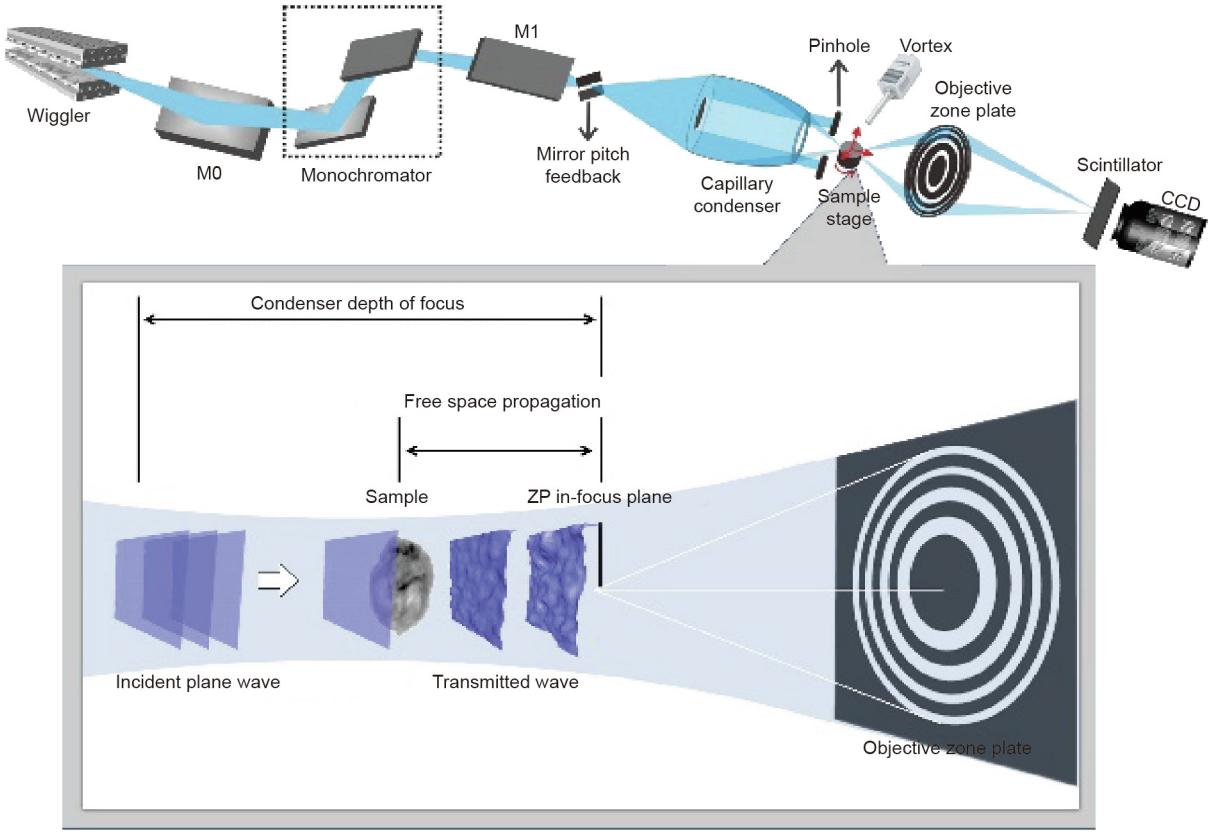

Fig. 11. Schematic drawing of proposed propagation-based X-ray phase contrast imaging using the nanoTXM system at beam line 6-2c at the SSRL.

large an angular access as possible, full 180° access is still unattainable, so the iterative method for processing incomplete 3D datasets will have to be implemented [25]. To reduce the background noise coming from the high-pressure sample environment, and especially from the supporting gasket, which is critical in phase retrieval, it will also be necessary to search for an optimized DAC-X-ray-propagation orientation and a gasket material for best performance.

5.3. Coherent diffraction imaging

Coherent XRD imaging (CDI) is a lens-less imaging technique that has been applied in the imaging of nanocrystalline and non-crystalline samples with nanoscale spatial resolution [47]. In theory, the spatial resolution of this technique is only limited by the X-ray wavelength. However, other factors including the diffraction power of the sample and the dynamic range of the detector result in additional constraints in practice. There are many different variations of CDI, each with specific pros and cons in different applications [48]. Bragg CDI has been applied at synchrotron sources to probe strain distribution in a gold (Au) nanoparticle compressed in a DAC in order to study the evolution of morphology and internal strain under high pressure with approximately 10 nm resolution [49]. The application of traditional CDI at third-generation synchrotron sources is limited in terms of the sample size that can be viewed due to the limitation of coherent lengths. Developments in X-ray ptychography represent an exciting future avenue, since this method permits the measurement of extended samples without the need to compromise spatial resolution. It is anticipated that continued developments in next-generation X-ray facilities, such as diffraction-limited storage rings [50] and X-ray free electron lasers [51], will further promote technical progress in the field of CDI imaging under high pressure. This would open up the visualization of samples under extreme conditions with unprecedented spatial and temporal resolution and lead to valuable insight and new discoveries in many scientific fields.

Acknowledgements

This work was supported by the Department of Energy (DOE) through the Stanford Institute for Materials & Energy Sciences (DE-AC02-76SF00515).

Compliance with ethics guidelines

Wendy L. Mao, Yu Lin, Yijin Liu, and Jin Liu declare that they have no conflict of interest or financial conflicts to disclose.

References

[1] Dubrovinsky L, Dubrovinskaia N, Bykova E, Bykov M, Prakapenka V, Prescher C, et al. The most incompressible metal osmium at static pressures above 750 gigapascals. Nature 2015;525(7568):226–9.
[2] Mao HK, Mao WL. Theory and practice—diamond-anvil cells and probes for high *P-T* mineral physics studies. In: Price GD, editor. Treatise on geophysics: mineral physics. Amsterdam: Elsevier; 2007. p. 231–68.
[3] Frankel RI. Centennial of Röntgen's discovery of X-rays. West J Med 1996;164(6):497–501.
[4] Du Plessis A, Le Roux SG, Guelpa A. Comparison of medical and industrial X-ray computed tomography for non-destructive testing. Case Stud Nondestr Test Eval 2016;6:17–25.
[5] Landis EN, Keane DT. X-ray microtomography. Mater Charact 2010;61(12):1305–16.
[6] Liu Y, Kiss AM, Larsson DH, Yang F, Pianetta P. To get the most out of high resolution X-ray tomography: a review of the post-reconstruction analysis. Spectrochim Acta B At Spectrosc 2016;117:29–41.
[7] Bautz W, Kalender W, Godfrey N. Hounsfield and his effect on radiology. Radiologe 2005;45(4):350–5. German.

[8] Sakdinawat A, Attwood D. Nanoscale X-ray imaging. Nat Photonics 2010;4(12):840–8.
[9] Chang C, Sakdinawat A. Ultra-high aspect ratio high-resolution nanofabrication for hard X-ray diffractive optics. Nat Commun 2014;5(1):4243.
[10] Shi CY, Zhang L, Yang W, Liu Y, Wang J, Meng Y, et al. Formation of an interconnected network of iron melt at Earth's lower mantle conditions. Nat Geosci 2013;6(11):971–5.
[11] Larabell CA, Nugent KA. Imaging cellular architecture with X-rays. Curr Opin Struct Biol 2010;20(5):623–31.
[12] Wei C, Xia S, Huang H, Mao Y, Pianetta P, Liu Y. Mesoscale battery science: the behavior of electrode particles caught on a multispectral X-ray camera. Acc Chem Res 2018;51(10):2484–92.
[13] Andrews JC, Weckhuysen BM. Hard X-ray spectroscopic nano-imaging of hierarchical functional materials at work. Chem Phys Chem 2013;14(16):3655–66.
[14] Meirer F, Cabana J, Liu Y, Mehta A, Andrews JC, Pianetta P. Three-dimensional imaging of chemical phase transformations at the nanoscale with full-field transmission X-ray microscopy. J Synchrotron Radiat 2011;18:773–81.
[15] Liu Y, Meirer F, Wang J, Requena G, Williams P, Nelson J, et al. 3D elemental sensitive imaging using transmission X-ray microscopy. Anal Bioanal Chem 2012;404(5):1297–301.
[16] Andrews JC, Almeida E, Van der Meulen MC, Alwood JS, Lee C, Liu Y, et al. Nanoscale X-ray microscopic imaging of mammalian mineralized tissue. Microsc Microanal 2010;16(3):327–36.
[17] Liu Y, Meirer F, Williams PA, Wang J, Andrews JC, Pianetta P. TXM-Wizard: a program for advanced data collection and evaluation in full-field transmission X-ray microscopy. J Synchrotron Radiat 2012;19(Pt 2):281–7.
[18] Gürsoy D, De Carlo F, Xiao X, Jacobsen C. TomoPy: a framework for the analysis of synchrotron tomographic data. J Synchrotron Radiat 2014;21:1188–93.
[19] Yang X, De Carlo F, Phatak C, Gürsoy D. A convolutional neural network approach to calibrating the rotation axis for X-ray computed tomography. J Synchrotron Radiat 2017;24:469–75.
[20] Yang Y, Yang F, Hingerl FF, Xiao X, Liu Y, Wu Z, et al. Registration of the rotation axis in X-ray tomography. J Synchrotron Radiat 2015;22(2):452–7.
[21] Guizar-Sicairos M, Boon JJ, Mader K, Diaz A, Menzel A, Bunk O. Quantitative interior X-ray nanotomography by a hybrid imaging technique. Optica 2015;2(3):259–66.
[22] Gürsoy D, Hong YP, He K, Hujsak K, Yoo S, Chen S, et al. Rapid alignment of nanotomography data using joint iterative reconstruction and reprojection. Sci Rep 2017;7(1):11818.
[23] Yu H, Xia S, Wei C, Mao Y, Larsson D, Xiao X, et al. Automatic projection image registration for nanoscale X-ray tomographic reconstruction. J Synchrotron Radiat 2018;25:1819–26.
[24] Liu Y, Wang J, Azuma M, Mao WL, Yang W. Five-dimensional visualization of phase transition in $BiNiO_3$ under high pressure. Appl Phys Lett 2014;104(4):043108.
[25] Wang JY, Yang W, Wang S, Xiao X, De Carlo F, Liu Y, et al. High pressure nano-tomography using an iterative method. J Appl Phys 2012;111(11):112626.
[26] Duan X, Yang F, Antono E, Yang W, Pianetta P, Ermon S, et al. Unsupervised data mining in nanoscale X-ray spectro-microscopic study of NdFeB magnet. Sci Rep 2016;6(1):34406.
[27] Xu Y, Hu E, Zhang K, Wang X, Borzenets V, Sun Z, et al. *In situ* visualization of state-of-charge heterogeneity within a $LiCoO_2$ particle that evolves upon cycling at different rates. ACS Energy Lett 2017;2(5):1240–5.
[28] Lin Y, Zeng Q, Yang W, Mao WL. Pressure-induced densification in GeO_2 glass: a transmission X-ray microscopy study. Appl Phys Lett 2013;103(26):261909.
[29] Zeng Q, Kono Y, Lin Y, Zeng Z, Wang J, Sinogeikin SV, et al. Universal fractional noncubic power law for density of metallic glasses. Phys Rev Lett 2014;112(18):185502.
[30] Liu H, Wang L, Xiao X, De Carlo F, Feng J, Mao HK, et al. Anomalous high-pressure behavior of amorphous selenium from synchrotron X-ray diffraction and microtomography. Proc Natl Acad Sci USA 2008;105(36):13229–34.
[31] Zeng Q, Lin Y, Liu Y, Zeng Z, Shi CY, Zhang B, et al. General 2.5 power law of metallic glasses. Proc Natl Acad Sci USA 2016;113(7):1714–8.
[32] Chen DZ, Shi CY, An Q, Zeng Q, Mao WL, Goddard 3rd WA, et al. Fractal atomic-level percolation in metallic glasses. Science 2015;349(6254):1306–10.
[33] Lin Y, Zhang L, Mao HK, Chow P, Xiao Y, Baldini M, et al. Amorphous diamond: a high-pressure superhard carbon allotrope. Phys Rev Lett 2011;107(17):175504.
[34] Lee SK, Lin JF, Cai YQ, Hiraoka N, Eng PJ, Okuchi T, et al. X-ray Raman scattering study of $MgSiO_3$ glass at high pressure: implication for triclustered $MgSiO_3$ melt in Earth's mantle. Proc Natl Acad Sci USA 2008;105(23):7925–9.
[35] Murakami M, Goncharov AF, Hirao N, Masuda R, Mitsui T, Thomas SM, et al. High-pressure radiative conductivity of dense silicate glasses with potential implications for dark magmas. Nat Commun 2014;5(1):5428.
[36] Petitgirard S, Malfait WJ, Sinmyo R, Kupenko I, Hennet L, Harries D, et al. Fate of $MgSiO_3$ melts at core-mantle boundary conditions. Proc Natl Acad Sci USA 2015;112(46):14186–90.
[37] Sato T, Funamori N. High-pressure structural transformation of SiO_2 glass up to 100 GPa. Phys Rev B Condens Matter Mater Phys 2010;82(18):184102.
[38] Wu M, Liang Y, Jiang JZ, Tse JS. Structure and properties of dense silica glass. Sci Rep 2012;2(1):398.
[39] Zha C, Hemley RJ, Mao H, Duffy TS, Meade C. Acoustic velocities and refractive index of SiO_2 glass to 57.5 GPa by Brillouin scattering. Phys Rev B Condens Matter 1994;50(18):13105–12.
[40] Sato T, Funamori N. Sixfold-coordinated amorphous polymorph of SiO_2 under high pressure. Phys Rev Lett 2008;101(25):255502.
[41] Murakami M, Bass JD. Spectroscopic evidence for ultrahigh-pressure polymorphism in SiO_2 glass. Phys Rev Lett 2010;104(2):025504.
[42] Williams Q, Jeanloz R. Spectroscopic evidence for pressure-induced coordination changes in silicate glasses and melts. Science 1988;239(4842):902–5.
[43] Stixrude L, Karki B. Structure and freezing of $MgSiO_3$ liquid in Earth's lower mantle. Science 2005;310(5746):297–9.
[44] Shen G, Mei Q, Prakapenka VB, Lazor P, Sinogeikin S, Meng Y, et al. Effect of helium on structure and compression behavior of SiO_2 glass. Proc Natl Acad Sci USA 2011;108(15):6004–7.
[45] Clark AN, Lesher CE, Jacobsen SD, Wang Y. Anomalous density and elastic properties of basalt at high pressure: reevaluating of the effect of melt fraction on seismic velocity in the Earth's crust and upper mantle. J Geophys Res Solid Earth 2016;121(6):4232–48.
[46] Ghosh DB, Karki BB, Stixrude L. First-principles molecular dynamics simulations of $MgSiO_3$ glass: structure, density, and elasticity at high pressure. Am Mineral 2014;99(7):1304–14.
[47] Jiang H, Xu R, Chen CC, Yang W, Fan J, Tao X, et al. Three-dimensional coherent X-ray diffraction imaging of molten iron in mantle olivine at nanoscale resolution. Phys Rev Lett 2013;110(20):205501.
[48] Miao J, Ishikawa T, Robinson IK, Murnane MM. Beyond crystallography: diffractive imaging using coherent X-ray light sources. Science 2015;348(6234):530–5.
[49] Yang W, Huang X, Harder R, Clark JN, Robinson IK, Mao HK. Coherent diffraction imaging of nanoscale strain evolution in a single crystal under high pressure. Nat Commun 2013;4(1):1680.
[50] Eriksson M, Van der Veen JF, Quitmann C. Diffraction-limited storage rings—a window to the science of tomorrow. J Synchrotron Radiat 2014;21:837–42.
[51] McNeil BWJ, Thompson NR. X-ray free-electron lasers. Nat Photonics 2010;4(12):814–21.